VNUHCM Journal of Science and Technology Development 2026, 29(2): 4051-4064

Open Access Full Text Article

Research Article

Conversion of rice husk ash into water-lubricated nanosilica hydrogel for brush coating on cellulose paper for water filtration

Hon Nhien Le*, Lam Nhu Pham, Thi Bich Duyen Luu, Thi Bang Tam Dao, Trung Do Nguyen, Thuc Chi Nhan Ha, Van Hieu Le*

ABSTRACT

In the Anthropocene context of water pollution by industrial chemicals and microplastics, the sustainable development of inexpensive, energy-saving, and biodegradable water purification membrane technologies is the urgent need for environmental remediation. While biodegradable cellulose filter papers are popular, cost-effective, and eco-friendly membrane materials, their large porous structure requires functional enhancement for effective microfiltration. Herein, we synthesized a nanosilica hydrogel (SG) via our chemical procedure of rice husk ash recycling. Silica nanoparticles derived from the SG hydrogel exhibited nanoscale particle sizes, suggesting that the hard agglomeration of stacked nanosilica powder is prevented by the hydration layers in the hydrogel structure. Notably, these hydration layers yielded water-lubricated silica nanoparticles for brush coating on cellulose filter substrates (Cell). The generated nanosilica/cellulose membranes (SG/Cell) were analyzed via top-view/cross-section scanning electron microscopy (SEM), energy-dispersive X-ray spectroscopy (EDS), X-ray diffraction (XRD), attenuated-total-reflectance Fourier-transform infrared spectroscopy (ATR-FTIR) and gas adsorption analyses of the surface areas and pore structures. The largely porous Cell substrate was significantly upgraded with SG coating to produce a more mesoporous membrane with a higher surface area and pore volume for aqueous microfiltration. Direct-flow filtration experiments revealed the high organic removal efficiency (88.4–99.7%) of the SG/Cell membranes under a hydraulic pressure of 0.01 bar, markedly outperforming regular cellulose membranes. In general, the SG/Cell membranes present the advantages of simplicity, low-pressure operation, cost-effectiveness, scalability, and environmentally friendly biodegradation. Brush coating cellulose filter papers with the water-lubricated nanomaterial hydrogel represents a promising approach in the preparation of practical water purification membranes.

Key words: rice husk ash, nanosilica hydrogel, hydration lubrication, cellulose filter paper, water filtration membrane

University of Science, VNUHCM, Vietnam

Correspondence

Hon Nhien Le, University of Science, VNUHCM, Vietnam

Email: lhnhien@hcmus.edu.vn

Correspondence

Van Hieu Le, University of Science, VNUHCM, Vietnam

Email: lvhieu@hcmus.edu.vn

History

- Received: 13-10-2025
- Revised: 29-12-2026
- Accepted: 30-12-2026
- Published Online: 02-06-2026

DOI : https://doi.org/10.32508/vnuhcmjstd.v29i2.4622

INTRODUCTION

In the 21st century, environmental pollution and climate change, driven by population growth, urbanization, and industrialization, have led to the globally pressing challenge of clean water scarcity.[1,2] With the microplastic and chemical contamination of rivers, oceans, and even rainwater, billions of people worldwide face daily water insecurity and health risks.[3–5]Conventional water treatment systems are often costly and energy intensive and, thus, limited in remote and poor regions. Sustainable developments addressing this crisis thus aim to produce effective, inexpensive, and biodegradable water filtration membrane materials. Such membranes should be capable of removing organic pollutants and pathogens from water with low energy consumption and reduced operational and environmental costs. Biodegradable cellulose filter papers represent practical, economical, and eco-friendly alternatives to nonbiodegradable and petroleum-derived polymer membranes currently used in industrial and societal activities. Derived from natural plant biomass, commercial cellulose filter membranes—porous scaffolds of cellulose fibers—are effective for wastewater treatment, laboratory experimentation, and household water purification.[6,7] The life cycle of cellulose-based membranes contributes to circular economy principles by integrating the renewable and biodegradable materials into ecological cycles.

In Vietnam, abundant agricultural rice husk constitutes a suitable renewable fuel for thermal energy generation in industrial boilers. Rice husk ash generated from the combustion process presents a rich silica source for nanosilica production.[8,9]The green recycling approach not only reduces the environmental burden of rice husk ash waste but also provides a rice-

Cite this article : Le H N, Pham L N, Luu T B D, Dao T B T, Nguyen T D, Ha T C N, Le V H. **Conversion of rice husk ash into water-lubricated nanosilica hydrogel for brush coating on cellulose paper for water filtration** *VNUHCM J. Sci. Technol. Dev.* 2026; 29(2):4051-4064

husk nanosilica alternative to the traditional energy-intensive production of silica from sand. Rice-husk-derived nanosilica exhibits a high surface area and porous structure and allows for the efficient adsorption of organic dyes, heavy metals, and other waterborne contaminants. The integration of biodegradable cellulose papers and rice-husk nanosilica represents an environmentally friendly strategy for developing affordable and sustainable water purification technologies.

Recent advances in nanosilica nanocomposite materials suggest that silica nanoparticles in hydrogel structures constitute a bioinspired approach to preventing the hard agglomeration of nanosilica powder,[10] a commonly observed issue when nanomaterials with a high surface area stack together.[11,12] Short interparticle distances lead to stronger van der Waals attractive forces, resulting in hard agglomerates; however, the re-dispersion of these in solvents to form nanoparticles is difficult. Our research on graphene-based materials has yielded the supramolecular hydration structure of water-intercalated hydrogels.[13–18] Another advantage of hydrogel structures is the natural lubrication of hydration layers between the nanostructures.[19–21] Hydration lubrication makes graphene-based hydrogels suitable for the direct brush coating of polymer substrates with graphene-based nanosheets.[13,14] Therefore, the intercalation of hydration layers in nanosilica hydrogels maintains interparticle distances, prevents hard agglomeration, and facilitates low-friction lubrication.[22–24] Nanosilica hydrogels showing no hard agglomeration constitute promising materials in the advanced preparation of nanostructured membranes for water filtration applications. The novelty lies in harnessing the hydration layers surrounding the silica nanoparticles to preserve the supramolecular nanosilica and create a hydration lubrication mechanism, opening a novel pathway for the simple brush coating of materials with nanostructured silica layers.

In this study, we used our eco-friendly procedure of recycling rice husk ash into nanosilica to prepare a nanosilica hydrogel.[8,9] The raw material (rice husk ash) and the target product (nanosilica hydrogel) were characterized to identify the material properties. Regular cellulose filter papers (Cell) were brush-coated with the water-lubricated nanosilica hydrogel (SG), yielding nanosilica/cellulose membranes (SG/Cell). The porous structure of the Cell paper was enhanced with the SG coating for water microfiltration purposes. Direct-flow filtration experiments were set up for testing the water purification performance. The SG/Cell membranes showed high removal efficiencies and ultrafast water permeance under a low hydraulic pressure of 0.01 bar. Thus, the brush-coated SG/Cell membrane represents a simple, inexpensive, and biodegradable structure for practical water filtration applications in industries, households, and even remote regions.

MATERIALS AND METHODS

Materials

Rice husk ash from industrial boilers was supplied by Star Tech Thermal Energy Company, Ho Chi Minh City, Vietnam. Potassium hydroxide (KOH) flakes and sulfuric acid (H_2SO_4; 95–98%) were purchased from Xilong Chemicals Company, methylene blue trihydrate (MB) was acquired from Xilong Scientific Company, and regular cellulose filter papers (diameter = 9 cm, medium flow rate) were obtained from New Star Company. Reverse-osmosis-purified water was used in the experiments.

Synthesis of nanosilica hydrogel from rice husk ash

Agricultural rice husks were burned in industrial boilers to supply renewable thermal energy. The residual rice husk ash was ground to produce fine rice husk ash for silica extraction using our clean production procedure.[8,9] First, the fine rice husk ash was dispersed in KOH solution (8%) at ~90 °C, and the black suspension was filtered through a membrane filter to separate the potassium silicate (K_2SiO_3) solution. After filtration, the potassium silicate solution was neutralized with acetic acid solution (15%) to achieve a solution pH of 7. The alkaline suspension and acetic acid formed a buffer solution in the neutral pH range, leading to the precipitation of silica nanoparticles stabilized by acetate coordination. The nanosilica precipitate was filtered and washed with excess water, yielding a clear hydrogel of precipitated nanosilica. After oven-drying at 80 °C to allow for gelation, the nanosilica hydrogel (SG) product was stored in a closed plastic container. Notably, the SG hydrogel was hydrated to a moisture content of ~95% (as measured by an electronic moisture analyzer).

Preparation of nanosilica/cellulose papers via brush coating with water-lubricated hydrogel

Regular cellulose filter papers were brush-coated with the as-synthesized SG hydrogel. First, a cellulose paper was placed on a glass Petri dish. A paintbrush was

then used to spread a thin, uniform layer of SG hydrogel on the cellulose paper, which was gently dried with a handheld dryer. The brush coating and hot air-drying processes were repeated four times, yielding a layer-by-layer nanosilica coating on the cellulose substrate. The nanosilica/cellulose membrane (SG/Cell) was then stored in a plastic bag before characterization and application.

Water filtration experiments

A direct-flow filtration system was set up using a standard glass filtration system, including a graduated funnel (diameter = 40 mm), a filter flask, and a clamp. In the water filtration experiments, a circular filter membrane was placed in the funnel, which was fixed with the clamp. The funnel was filled with aqueous solutions such that the height from the filter membrane to the water surface was 102 mm. The height of the water level was equivalent to a hydraulic pressure of 102 mmH_2O (~0.01 bar), which was maintained during the experiments. Therefore, the transmembrane pressure was kept constant at 0.01 bar, and the surface area of the filtration membrane was approximately 12.57 cm^2. By measuring the filtrate volume and filtration time, the water permeance or water flux through the membrane was calculated, as in Equation 1:

$$F = \frac{V}{(A \times T \times P)} \quad (1)$$

where F is the water flux or filtrate permeance (L h^{-1} m^{-2} bar^{-1}), V is the filtrate volume (L) passing through the membrane area A (m^2) over filtration time T (h), and P is the transmembrane pressure (bar).

MB was dissolved in water to obtain dye concentrations of 1 ppm (MB1) and 20 ppm (MB20). In the water filtration experiments, water and the MB1 and MB20 solutions were passed through the regular (Cell) and nanosilica-coated (SG/Cell) cellulose membranes. The filtrate solutions were analyzed via UV-Vis spectroscopy to determine the MB concentrations. The absorbance at a wavelength of 665 nm was recorded to calculate the MB concentrations using the standard calibration equation $y = 0.1735x$(R^2 = 0.9988) in the MB concentration range of 0 - 10 ppm.

Typically, the glass funnel was filled with an MB solution (hydraulic transmembrane pressure = 102 mmH_2O or 0.01 bar), and the water filtration experiments lasted 15 minutes. The filtrate was collected and analyzed using weight measurements and UV-Vis spectroscopy. The dye removal efficiency was calculated according to Equation 2:

$$RE(\%) = \frac{C_0 - C}{C_0 \times 100\%} \quad (2)$$

where RE (%) is the dye removal efficiency of the filtration membrane, C_0 (ppm) is the dye concentration in the initial input solution, and C (ppm) is the dye concentration in the filtrate.

Analytical instrumentation

The weight of the materials and the moisture content of the hydrogels were measured using an Ohaus Pioneer balance and an A&D MX-50 moisture analyzer, respectively. The microstructures of the nanoparticles were visualized with a scanning electron microscopy (SEM) system (JEOL JSM-IT200) equipped with an energy-dispersive X-ray spectroscopy (EDS) instrument for elemental analysis. The as-prepared membranes were characterized via X-ray diffraction (XRD) using a Bruker D8 Advance diffractometer. The nanosilica-coated membranes were analyzed via attenuated-total-reflectance Fourier-transform infrared (ATR-FTIR) spectroscopy using a Thermo Scientific Nicolet 6700 infrared spectrometer. The UV-Vis spectra of the aqueous solutions were measured using a Jasco V-730 instrument. A Quantachrome Nova instrument (Anton Paar) was employed for the gas adsorption analyses (nitrogen gas adsorption at 77 K). Samples of the filtration membranes were cut into small pieces (approximately 3 × 3 mm) and outgassed at 80 °C for at least 2 hours before the gas adsorption measurements. Brunauer–Emmett–Teller (BET) theory, Barrett–Joyner–Halenda (BJH) model, and density functional theory (DFT) calculations were used for the data analysis using Quantachrome NovaWin software.

RESULTS AND DISCUSSION

Conversion of boiler rice husk ash into water-lubricated nanosilica hydrogel

Today, agricultural rice husk represents a renewable biomass fuel for industrial boilers and thermal power plants that generate thermal energy. Our previous work revealed that boiler rice husk ash is rich in silica, with ~70 wt% silicon, ~18 wt% carbon, ~8 wt% potassium, ~1.5 wt% calcium, ~0.66 wt% aluminum, ~0.41 wt% manganese, ~0.26 wt% sulfur, ~0.2 wt% phosphorus, and ~0.2 wt% iron.[8] Elemental mapping via microscopic X-ray fluorescence (micro-XRF) spectroscopy revealed a relatively uniform distribution of silicon throughout the ash matrix and specific regions of potassium. The high contents of silicon, carbon, and potassium suggest that rice husk

ash is a significant resource for silica extraction, biocarbon production, and potassium fertilizer manufacturing. Notably, residual rice husk ash from industrial boilers has been converted into silica nanomaterials, biocarbon products, and potassium fertilizers using our innovative recycling technology.[9] While conventional recycling processes employ sodium hydroxide (NaOH) solution to extract silica and sulfuric acid to neutralize sodium silicate and precipitate nanosilica, our method uses a potassium hydroxide (KOH) solution. Compared with the traditional NaOH approach, the use of KOH presents several advantages: KOH exhibits strong alkalinity for silica extraction and activated carbon production, and wastewater containing K^+ cations is useful for producing potassium macronutrient and foliar fertilizers. The recycling protocol was designed to address the critical issue of wastewater pollution by utilizing the potassium salts in wastewater for agricultural fertilizers. Therefore, the KOH method presents the advantages of clean production, high productivity, a circular economy, and environmental sustainability.

Herein, rice husk ash (Figure 1a) was ground into a fine powder and analyzed via SEM. The microstructures of the fine rice husk ash (SEM images in Figures 1b and 1c) reveal porous morphologies, with particle sizes of approximately 100 μm. The porous structure results from the pyrolysis of organic components in the rice husk during combustion in the boiler. The porous network of inorganic carbon and silica was analyzed via EDS for elemental composition characterization (Table 1). The rice husk ash contains four main elements: carbon (C), oxygen (O), silicon (Si), and potassium (K). The quantitative EDS data reveal elemental contents of 69.46 at% C (58.48 wt%), 23.33 at% O (26.16 wt%), 5.70 at% Si (11.22 wt%), and 1.51 at% K (4.15 wt%). As the EDS analysis focused on the region of the carbon framework, a high carbon proportion was detected, leaving the silica proportion at approximately 33.66 wt%. The carbon content is attributed to pyrolyzed carbon and some unburned organic matter.

After the recycling process using the KOH solution, nanosilica was precipitated as a product. Nanosilica in the form of a fine powder has been characterized in our previous study, exhibiting an amorphous silica structure (broad XRD peak at $2\theta \approx 21$–23°) and high purity (EDS elemental contents of 29.44 at% Si and 66.93 at% O).[8] Nanosilica surfaces are hydrophilic, with silanol groups (Si–OH) and siloxane groups (Si–O–Si), as identified in the FTIR spectra. Hydrogen bonding between silanol groups and water molecules leads to the hydration and dispersibility of silica nanoparticles in aqueous solutions. However, the hard agglomeration of silica nanoparticles occurs during the drying process. During solvent evaporation, capillary forces from menisci pull the nanoparticles together, increasing van der Waals attractive forces over short distances. The hydrogen bonds between silanol groups and the van der Waals attractive forces become significant and induce the hard agglomeration of silica nanoparticles. Furthermore, condensation reactions of the silanol groups may occur to form Si–O–Si covalent bonds, making the agglomeration irreversible.

In the SG hydrogel (Figure 1d), a high moisture content (~95%) is essential to retain the hydration layers on the SG nanoparticles. The hydration layers are not only intercalated in the hydrogel to maintain the spacing between the nanoparticles but also lead to hydration lubrication. After the slow evaporation of water molecules, SEM images of the hydrogel (Figures 1e and 1f) reveal the nanostructures of the SG agglomerates. Although the dry SG nanoparticles agglomerated to form a porous morphology, the particle sizes of distinct SG nanoparticles are estimated to be below 50 nm. The particle sizes of the nanosilica in the SG hydrogel are considerably smaller than those of fine nanosilica powder (~50 nm).[8] In addition, the elemental composition of the SG nanosilica involves 23.56 at% Si and 76.44 at% O (with the EDS results presented in Table 1). The atomic ratio of O/Si is ~3.2, which is higher than the theoretical ratio of 2 in the molecular formula of SiO_2. It is believed that water molecules trapped among the SG particles and silanol groups on the SG surfaces account for the additional O content in the structure.

Brush coating of cellulose papers with nanosilica hydrogel to yield nanostructured membranes

Recent studies have reported significant progress in the preparation of nanosilica/cellulose nanocomposite membranes for water purification applications through improvements in adsorption, fouling resistance, and separation performance. Kumarage et al. (2023) developed electrospun cellulose acetate membranes embedded with amine-functionalized silica nanoparticles. The large surface area and functionalized surface of the nanosilica in the hydrophilic cellulose matrix resulted in the high adsorption of metal cations in hard water (Ca^{2+} and Mg^{2+}) and heavy metals in polluted water (As^{5+}, Cd^{2+}, and Pb^{2+}).[25] Another study described the incorporation of mesoporous silica into nanofibrillated cellulose

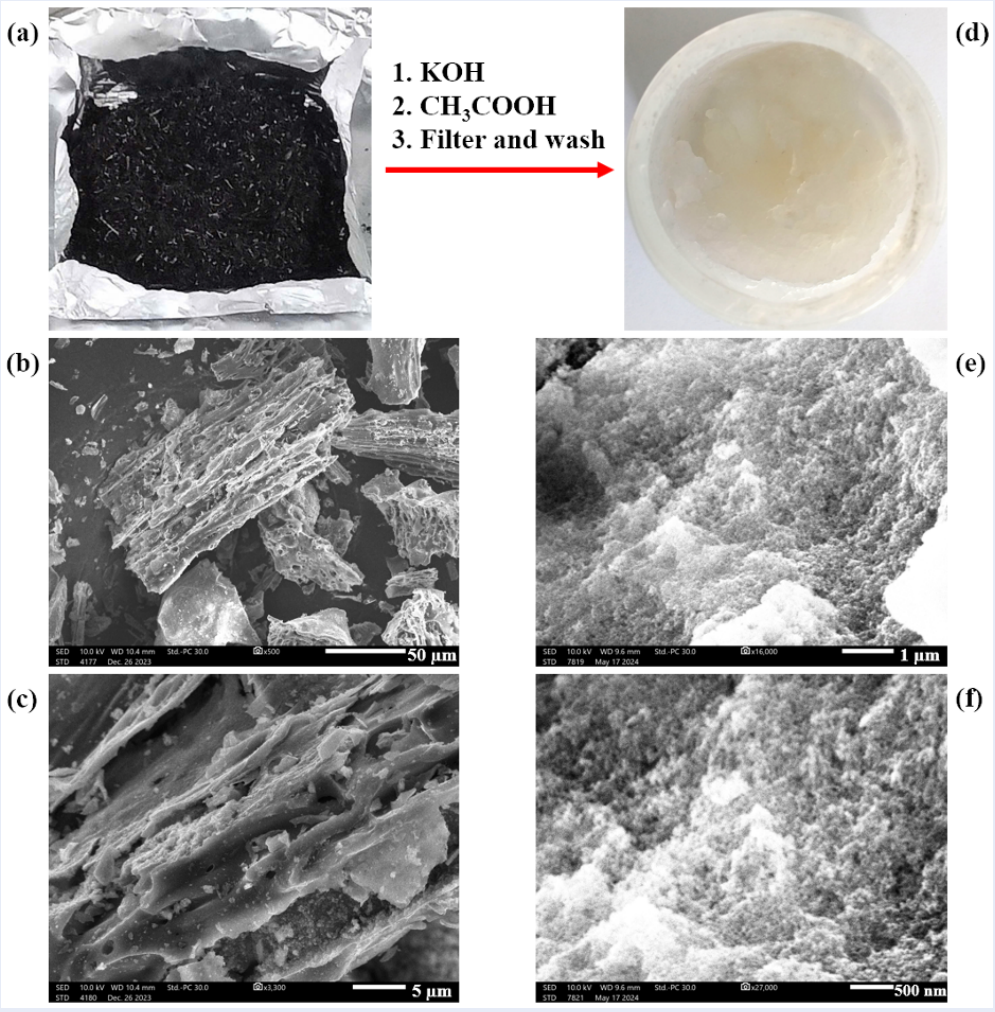

Figure 1: (a) Rice husk ash, and SEM images of its structure using scale bars of (b)50 μm and (c) 5 μm. (d) Nanosilica hydrogel, and SEM images of its nano structure at scale bars of (e) 1 μm and (f) 500 nm.

Table 1: EDS elemental analysis of rice husk ash and nanosilica hydrogel (SG). Elemental contents of SG was referenced from our previous paper [13].

Materials	Si (atom %)	O (atom %)	C (atom %)	K (atom %)
Rice husk ash	5.70 ± 0.28	23.33 ± 0.91	69.46 ± 0.96	1.51 ± 0.19
SG	23.56 ± 1.36	76.44 ± 2.79	-	-

membranes, yielding high adsorption capacities for organic dyes and heavy metal ions in water treatment applications.[26] Moreover, ultrafiltration membranes based on microfibrillated cellulose scaffolds integrated with silica nanoparticles exhibit low fouling, a high water flux, and a high separation efficiency (~99.6%) compared to commercial ultrafiltration membranes.[27] Further, Ali et al. (2022) fabricated nanocomposite membranes of cellulose acetate and silica nanoparticles via a phase inversion process for desalination applications, which showed an enhanced water flux compared to pristine cellulose acetate membranes.[28] Their results highlight the role of nanosilica in increasing hydrophilicity and water transport pathways through cellulose-based membranes.

According to the literature, silica nanoparticles also promote regimes of very low friction (superlubricity) in aqueous ceramic lubrication systems.[29–31] Dispersed hydrated nanosilica fills grooves and creates

smooth interfaces for ultralow friction. Regarding the SG hydrogel in this study, hydration lubrication is beneficial in preventing the stacking of silica nanoparticles and allowing them to slide over each other smoothly; this is not achievable with hard agglomerates in stacked nanosilica powder. The hydration lubrication of nanosilica hydrogels represents a simple approach to the low-friction movement of hydrated silica nanoparticles by exploiting the hydration shells around the non-stacked nanoparticles. The reversible hydrogen bonding of water molecules and hydrophilic nanomaterial surfaces enables smooth sliding under mechanical loads.[32] Therefore, the SG hydrogel was water-lubricated for the direct brush coating of cellulose substrates. Thin nanosilica coatings were brush-coated layer by layer onto the cellulose filter paper (Cell, Figure 2a), producing the SG/Cell membrane (Figure 2b).

The XRD pattern of the SG/Cell paper (Figure 2c) reveals the characteristic peaks of cellulose structures in the Cell membrane, specifically at 2θ = 15°, 16.5°, 20.8°, and 22.9°. A typical broad peak of amorphous SG arises at around 2θ = 22°,[8] but the signal overlaps with the peaks of the cellulose substrate in the XRD pattern. The SG coating on the Cell substrate was analyzed via ATR-FTIR spectroscopy to identify the chemical groups on the surface of the SG/Cell membrane. In the FTIR spectrum (Figure 2d), the bands at 628, 791, and 1051 cm^{-1} correspond to the symmetric bending, symmetric stretching, and asymmetric stretching of the siloxane group (Si–O–Si) in the SG coating, respectively.[31] The FTIR peaks at 2898 and 2972 cm^{-1} are assigned to stretching vibrations of C–H bonds in the cellulose substrate.[33]

The porous network of cellulose fibers is filled with the brush-coated layer of silica nanoparticles. The top-view SEM images in Figures 3a–3c depict the nanostructures of the SG/Cell surfaces. Possessing nanoscale particle sizes (< 50 nm), the nanosilica in the SG hydrogel enters the porous scaffold of the underlying cellulose membrane during the brush coating process. The nanosilica surfaces, containing hydrophilic silanol groups, are compatible with the hydroxyl-group-rich structures of the cellulose fibers, leading to the formation of a porous SG/Cell network (SEM images in Figures 3a and 3b). The average pore sizes of the cellulose filter paper fall in the range of 15–20 μm (specified by the supplier), which is sufficient for the removal of coarse particles, such as sand, silt, and plant fibers. The SG coating on the cellulose fiber network significantly reduces the pore sizes to below 10 μm, which is in the range of microfiltration membranes (10 nm to 10 μm).[34] The simple brush coating of the water-lubricated SG hydrogel improved the porosity of regular cellulose filter papers to form a nanostructured SG/Cell network for microfiltration applications.

The results of further EDS analysis on the SG coating area (SEM image in Figure 3c) are presented in the EDS spectrum in Figure 3d and the elemental composition table in Figure 3e. Accordingly, the three main elements of Si, O, and C correspond to silica (SiO_2) and cellulose ($C_6H_{10}O_5$) in the SG/Cell structure. According to the EDS results, the atomic proportions of Si, O, and C are 24.01, 49.81, and 26.19%, respectively. Silica (with a content of ~72%) is dominant in the area, and the carbon and oxygen contents of cellulose account for the remaining elemental composition (~28%). The elemental composition also indicates that the SG/Cell membrane is composed of an upper SG coating and a lower Cell substrate.

The cross-sectional SEM images in Figure 4 provide more detailed views of the SG/Cell membrane architecture, indicating a thin SG coating on a thick Cell substrate. As shown in Figures 4a and 4b, the Cell structure includes interconnected cellulose fibers, with large diameters in the range of 15–20 μm. The thickness of the Cell substrate is estimated to be approximately 180 μm. Figures 4c and 4d present higher-resolution images of the SG coating, comprising a porous structure of agglomerated silica nanoparticles. While the SG coating above the Cell substrate displays a thickness of up to 5 μm, SG nanoparticles also penetrate and occupy the upper portion of the Cell substrate. Brush coating represents a simpler and faster technique compared to vacuum filtration with regard to the dispersion of nanomaterials for coating cellulose filter substrates.[35,36] The brush coating process also reveals the promising application potential of the SG hydrogel in waterborne coating systems, where nanosilica contributes to improved mechanical and barrier properties.[37–39]

Gas adsorption analysis of surface areas and pore structures of filtration membranes

The Cell and SG/Cell membranes were analyzed using nitrogen gas adsorption tests at 77 K (Figure 5). The adsorption–desorption isotherm data of the Cell (Figure 5a) and SG/Cell (Figure 5b) membranes reveal type-V isotherms and type-H4 hysteresis loops, based on International Union of Pure and Applied Chemistry (IUPAC) classifications.[40] The isotherms indicate a mesoporous structure (pore size of 2–50 nm), capillary condensation, and weak adsorbate–adsorbent interactions. Despite the weak interactions

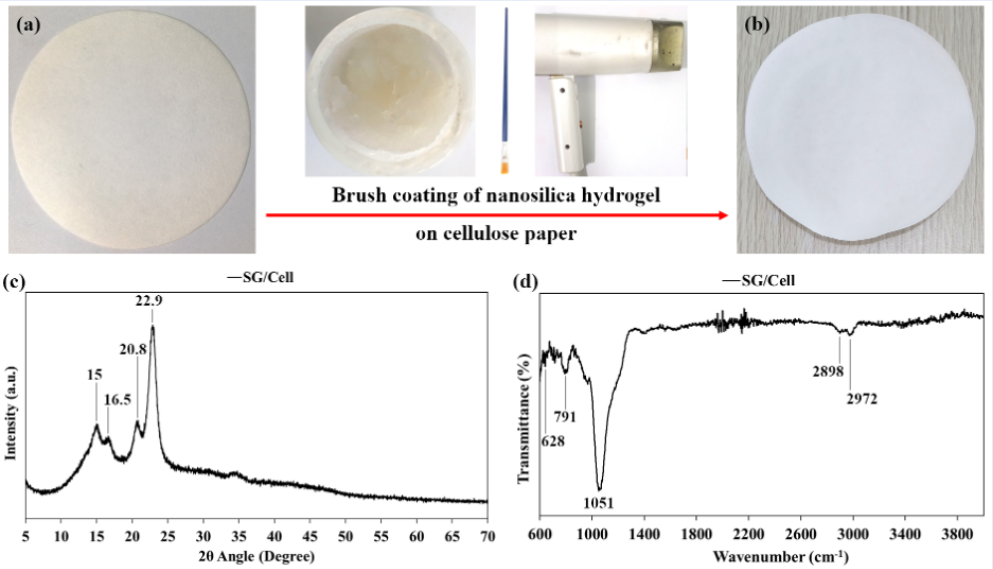

Figure 2: Brushcoating of water-lubricated nanosilica hydrogel onto cellulose paper using abrush and a handheld dryer. (a) Initial cellulose paper, (b) brush-coatedSG/Cell paper, (c) XRD pattern of the SG/Cell paper, and (d) ATR-FTIR spectrum of the SG coating on the cellulose substrate.

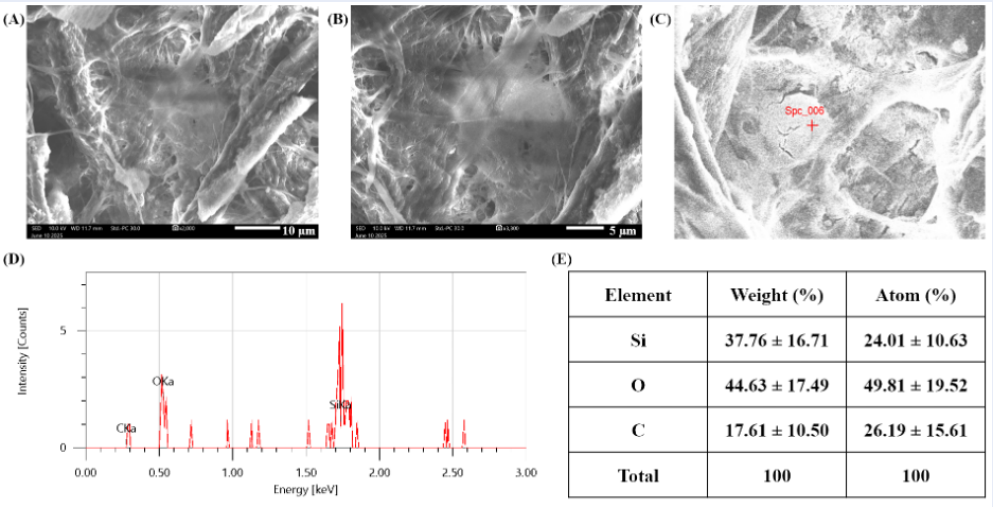

(E)

Element	Weight (%)	Atom (%)
Si	37.76 ± 16.71	24.01 ± 10.63
O	44.63 ± 17.49	49.81 ± 19.52
C	17.61 ± 10.50	26.19 ± 15.61
Total	100	100

Figure 3: Top-view SEM images of the SG/Cell paper (SG coating on a network ofcellulose fibers) with scale bars of (a) 10 μm and (b) 5 μm. SEM-EDS analysis: (c)SEM image of SG coating area, (d) EDS spectrum, and (e) elemental compositions of Si, O, and C.

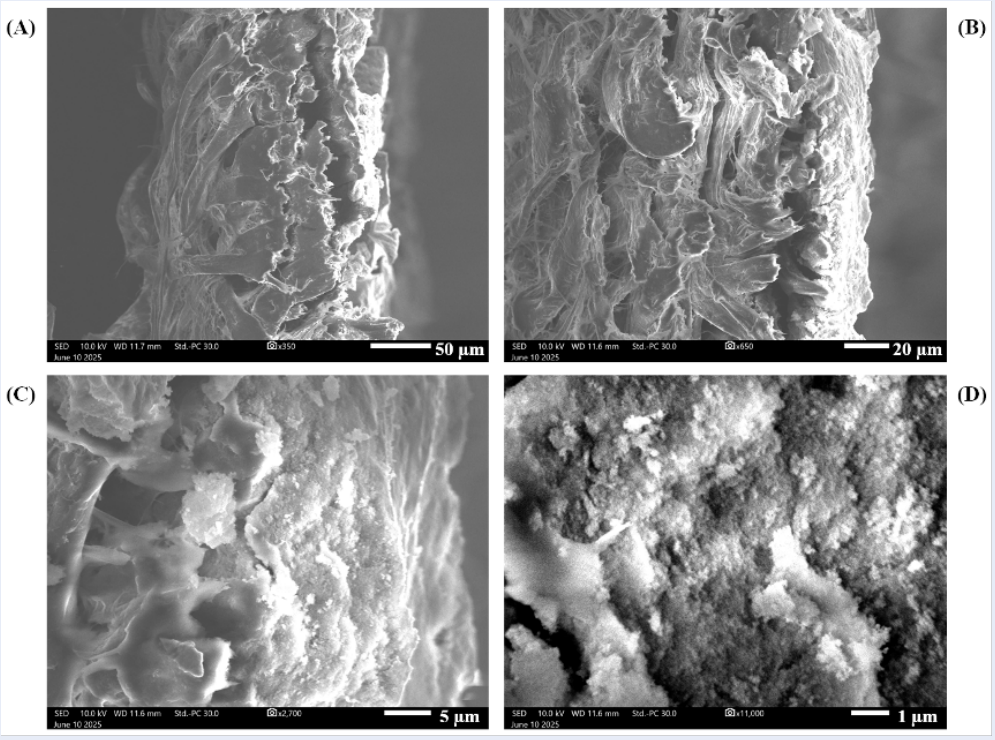

Figure 4: Cross-sectional SEM images of the SG/Cell paper, with scale bars of (a) 50 μm, (b) 20 μm, (c) 5μm, and (d) 1 μm.

and hysteresis loops in the isotherms, BET theory, BJH model, and DFT calculations can be applied to determine the specific surface areas and pore structure distributions.

According to the pore volume distributions (dV-BJH) in Figure 5c, the Cell membrane exhibits the highest pore volume (~0.0014 cm^3 g^{-1}) at a pore width of 2.721 nm, and the SG/Cell membrane displays the optimal pore volume (~0.0035 cm^3 g^{-1}) at a pore width of 1.427 nm. As presented in Figure 5c and Table 2, the cumulative pore volume (V-BJH) of SG/Cell (0.022 cm^3 g^{-1}) is 2.75-fold higher than the value of Cell (0.008 cm^3 g^{-1}). With a higher total pore volume, the SG/Cell membrane also exhibits a larger specific surface area (8.249 m^2 g^{-1}), 2.44-fold higher than that of the Cell membrane (with the BET surface areas presented in Table 2). The large pore structure of the substrate is fouled with coating nanoparticles, resulting in an increase in the surface area and a decrease in the pore width.[41] The brush-coated SG layer on the Cell substrate increases the microporosity of the membrane to yield a larger surface area and a higher pore volume.

In addition, Figure 5d presents DFT calculations of the pore volume distributions and cumulative pore volumes of the filtration membranes. The DFT method—specifically, the non-local DFT (NLDFT) model of nitrogen adsorption on silica at 77 K—was employed to analyze the surface areas and pore structures, generating reference results of the specific surface areas, pore volumes, and pore widths of the mesoporous solids with surface roughness. As shown in Table 2, the DFT surface area of SG/Cell (6.237 m^2 g^{-1}) is 2.55-fold larger than that of Cell (2.449 m^2 g^{-1}). Notably, the cumulative pore volume of SG/Cell (0.018 cm^3 g^{-1}) is triple that of Cell (0.006 cm^3 g^{-1}). The DFT calculations further support the values of the surface areas and pore structures generated via the BET and BJH methods. In both the BET/BJH methods and DFT calculations, similar trends of an increasing surface area and pore volume and a decreasing pore width confirm that the SG coating plays an important role in narrowing the pore size for molecular sieving and enhancing the pore volume and surface area for molecular adsorption.

Direct-flow water filtration experiments

Direct-flow water filtration presents several advantages, such as simplicity, cost-effectiveness, and efficiency, in the context of certain applications. As-

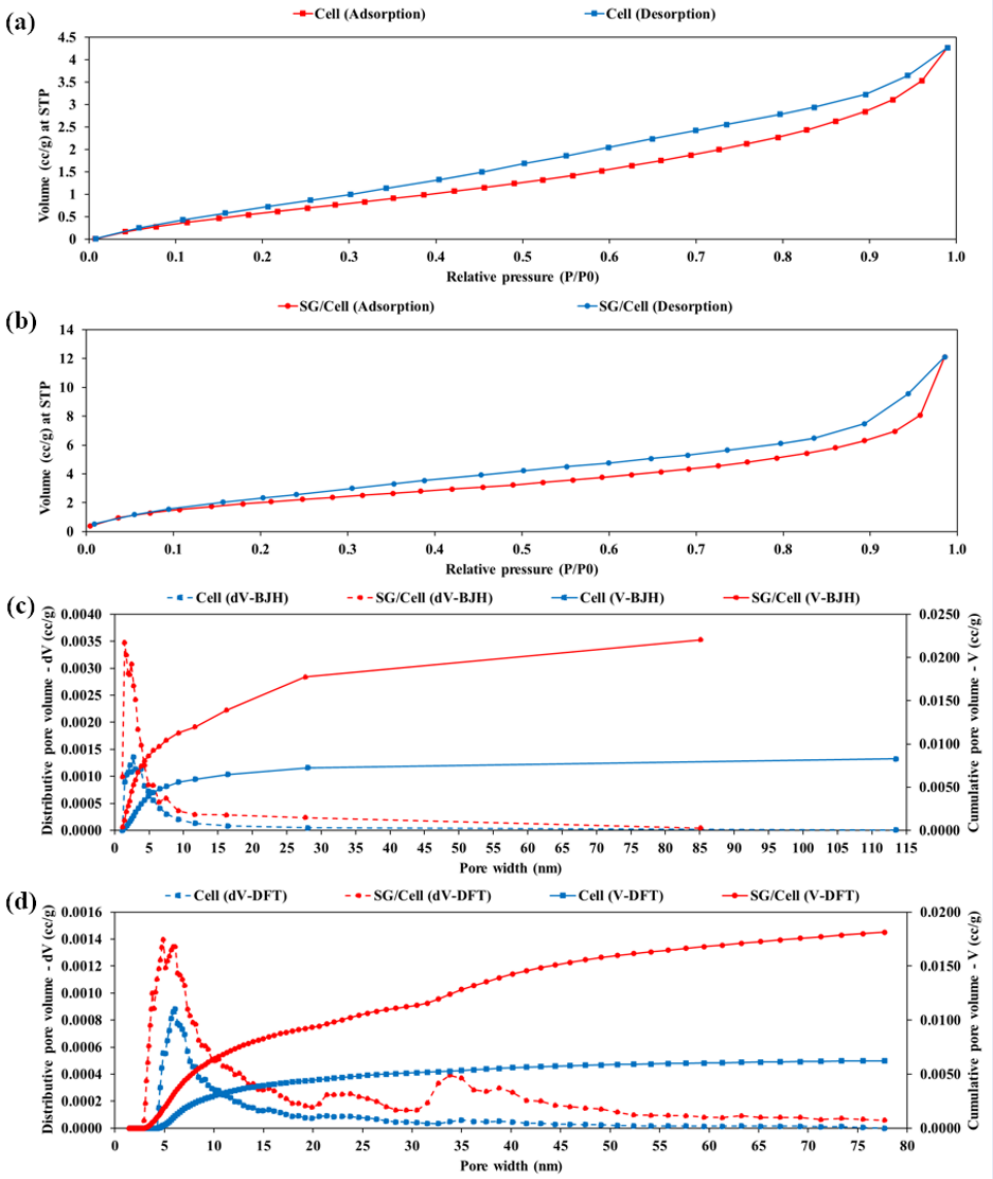

Figure 5: Nitrogen adsorption–desorption isotherms at 77 Kfor the (a) Cell membrane and (b) SG/Cell membrane. (c) Pore volume distributions (dV-BJH) and cumulative pore volumes (V-BJH) obtained from the BJH model. (d) Pore volume distributions (dV-DFT) and cumulative pore volumes (V-DFT) calculated from NLDFT model of nitrogen adsorption on silica at 77 K.

prepared direct-flow filtration systems are depicted in Figures 6a and 6b, including a 300-mL glass funnel, a clamp for fixing the filtration membranes in place, and a glass flask for capturing the filtrates. After fixing the filter membranes in place using the funnel and clamp, aqueous solutions were added to the funnel up to the maximum water level to maintain a hydraulic pressure of 102 mmH_2O, or 0.01 bar (with a height of 102 mm from the membrane to the water surface). Pure water, MB1 (1 ppm, Figure 6a), and MB20 (20 ppm, Figure 6b) were investigated in the experiments. The filtrate solutions were analyzed via UV-Vis spectroscopy to determine the MB concentrations and the dye removal efficiencies. The UV-Vis spectra in Figure 6c show characteristic signals of MB molecules, notably the absorption peak at 665 nm. The spectra indicate that very small amounts of MB molecules remain in the filtrates after filtration

Table 2: Summary of specific surface areas and pore structures of the Cell andSG/Cell membranes.

Gas adsorption analysis	Cell membrane	SG/Cell membrane
BET surface area (m^2 g^{-1})	3.376	8.249
BJH pore volume (cm^3 g^{-1})	0.008	0.022
BJH pore width (nm)	2.721	1.427
DFT surface area (m^2 g^{-1})	2.449	6.237
DFT pore volume (cm^3 g^{-1})	0.006	0.018
DFT pore width (nm)	6.079	4.887

through the SG/Cell membranes; furthermore, the dye removal efficiencies (99.7% for MB1 and 88.4% for MB20) are sufficiently high for practical applications.

The water permeances and removal efficiencies of the Cell and SG/Cell membranes are presented in Figures 6d and 6e. While the flux of clean water through a regular cellulose filter is 1642.16 L h^{-1} m^{-2} 0.01bar^{-1}, the clean water permeance through an SG/Cell membrane is 777.31 L h^{-1} m^{-2} 0.01bar^{-1}. Although the brush-coated SG layer significantly reduces the water flux, the permeance of 777.31 LMH is considered a good value in comparison with high-pressure microfiltration systems (240–1400 LMH, Table 3).[42–45] Notably, both the Cell and SG/Cell membranes exhibit significant decreases in water flux in the MB1 and MB20 filtrations. The water permeances through the Cell paper are 1642.16 LMH for clean water, 769.99 LMH for MB1, and 460.59 LMH for MB20. A similar declining trend in the water flux was observed in the direct-flow filtration using the SG/Cell membranes. The permeances of water, MB1, and MB20 through the SG/Cell membrane are 777.31, 242.79, and 178.09 LMH, respectively. The adsorption of MB molecules onto the membranes leads to organic fouling and clogging, which are responsible for the decrease in water permeance compared to clean water filtration.

Regarding the water purification performances, the adsorption and fouling of the MB dyes on the Cell filters benefited the dye removal efficiencies (15% for MB1 and 9% for MB20). Small proportions of MB were removed by the regular Cell papers under the low transmembrane pressure of 0.01 bar. The dye removal efficiencies of the SG/Cell membranes are satisfactory, with values of 99.7% for MB1 and 88.4% for MB20. The mechanism of MB removal is attributed to the nanostructured SG coating and the effective MB adsorption capacity of the SG/Cell membrane. The brush-coated nanosilica layer significantly improves the structure of the SG/Cell membrane, which exhibits a smaller pore structure (mesopore width = 2–50 nm), a higher pore volume (0.022 cm^3 g^{-1}), and a larger surface area (8.249 m^2 g^{-1}). In addition, nanosilica is effective for MB adsorption, with fast adsorption kinetics, rapidly reaching equilibrium due to the electrostatic attraction between the negatively charged nanosilica surface and the cationic MB molecules.[46] Miri et al. demonstrated that the nanocomposite membrane comprising mesoporous silica and nanofibrillated cellulose exhibits strong MB adsorption (~1160 mg m^{-2}) in water purification experiments.[26] Therefore, in the case of the nanostructured SG/Cell membrane, MB adsorption and fouling mechanisms contribute to the favorable water filtration efficiency.

Overall, the brush-coated SG/Cell membrane attains a dye removal efficiency of above 88% for the MB solutions under a hydraulic pressure of 0.01 bar. As shown in Table 3, the water purification performance is comparable to that of microfiltration systems operating at high pressures for the removal of microplastic particles, organic matter, and biological structures from water.[42–45] While direct-flow filtration through the SG/Cell membranes cannot sustain high removal efficiencies under high pressures (~1 bar), implementing the SG/Cell filtration system under a low hydraulic pressure (~0.01 bar) presents a simple and useful option for household application, portable filtration, remote scenarios, and pre-filtration before advanced treatments such as nanofiltration and reverse osmosis.

CONCLUSION

To summarize, rice husk ash was converted into a nanosilica hydrogel (SG hydrogel) using the chemical processes of silica extraction in potassium hydroxide solution and silica precipitation in acetic acid solution. The precipitated silica nanoparticles

Table 3: Summary of water permeances and removal efficiencies of cellulose-basedmembranes in this study and other microfiltration membranes in the literature.

Membrane materials and water filtration performances		Pure water	Water containing methylene blue	Water containing microplastic particles (~10 μm)	Water containing sucrose	Water containing bovine serum albumin
Regular cellulose membrane (*)	Permeance (L h^{-1} m-2 0.01bar^{-1})	1642.16	460.59–769.99	-	-	-
	Removal efficiency (%)	-	9–15	-	-	-
Brush-coated SG/Cell membrane (*)	Permeance (L h^{-1} m-2 0.01bar^{-1})	777.31	178.09–242.79	-	-	-
	Removal efficiency (%)	-	88.4–99.7	-	-	-
Polyethylene oxide/ bentonite/ polyaniline membrane [42]	Permeance (L h^{-1} m-2 bar^{-1})	-	240–380	-	-	-
	Removal efficiency (%)	-	83–85	-	-	-
5-μm Durapore membrane [43]	Permeance (L h^{-1} m^{-2})	-	-	250–1000	-	-
	Removal efficiency (%)	-	-	99	-	-
0.45-μm Durapore membrane [43]	Permeance (L h^{-1} m^{-2})	-	-	250–1000	-	-
	Removal efficiency (%)	-	-	100	-	-
Polyethersulfone (PES) membrane [44]	Permeance (L h^{-1} m-2 bar^{-1})	1130–1442	-	-	-	-
	Removal efficiency (%)	-	-	-	64–83	-
Polydopamine-coated PES membrane [44]	Permeance (L h^{-1} m^{-2} bar^{-1})	1180–1340	-	-	-	-
	Removal efficiency (%)	-	-	-	85–95	-
Sulfonated polyethersulfone (SPES)	Permeance (L h^{-1} m^{-2} bar-^{1})	440	-	-	-	-
	Removal efficiency (%)	-	-	-	-	90
SPES mixed with 5–10% metal–organic frameworks [45]	Permeance (L h^{-1} m^{-2} bar^{-1})	487–565	-	-	-	-
	Removal efficiency (%)	-	-	-	-	~95

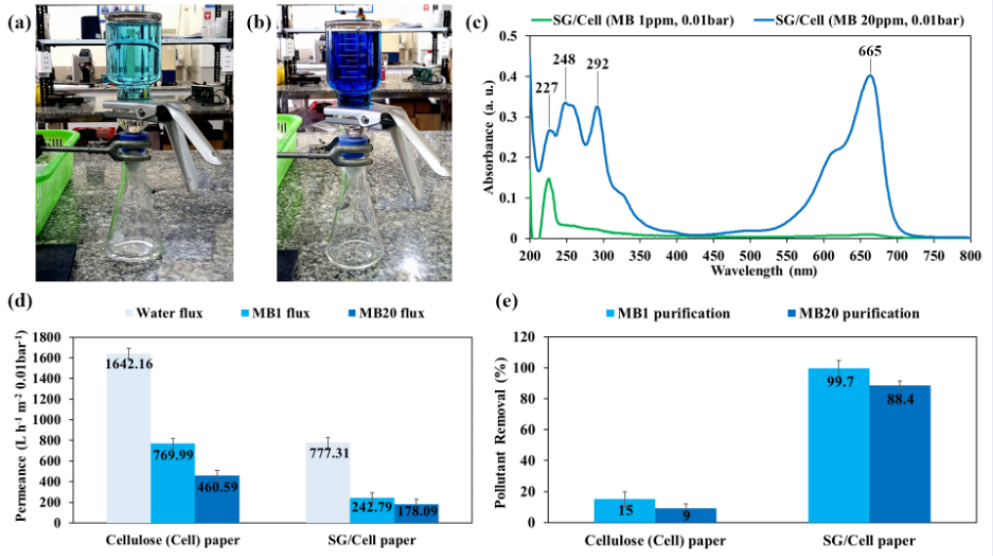

Figure 6: (a, b) Experimental water filtration setups with methylene blue solutionsMB1 (1 ppm) and MB20 (20 ppm). (c) UV-Vis spectra of MB1 and MB20 solutions after filtration through SG/Cell papers at the hydraulic transmembrane pressureof 0.01 bar. (d) Water fluxes (water permeances) through the Cell and SG/Cellpapers. (e) Dye removal efficiencies of the Cell and SG/Cell papers.

were hydrated and preserved in the hydrogel structure. As the SG hydrogel contained distinct nanoparticles separated and lubricated by hydration boundary layers, the layer-by-layer brush coating of the water-lubricated SG hydrogel produced nanostructured silica coatings on cellulose filter papers. The thin SG coating penetrated and built up the upper layer of the SG/Cell membrane, resulting in a more mesoporous structure with a larger surface area and higher pore volume. Direct-flow water filtration experiments on the Cell and SG/Cell papers demonstrated that the nanosilica coating enhanced the performance of the cellulose-based membranes with regard to the microfiltration of organic dyes in water. Under the hydraulic transmembrane pressure of 0.01 bar, a high water purification performance, with a dye removal efficiency of 88.4–99.7%, was achieved. The SG/Cell membranes are also eco-friendly because Cell substrates constitute biodegradable organic matter, and SG coatings comprise secondary silicon nutrients for agricultural plants. Environmentally friendly materials, simple synthetic processes, and effective water filtration performances make brush-coated nanosilica/cellulose membranes a practical option for portable, household, and even industrial water purification applications.

ACKOWLEDGEMENTS

This research is funded by Vietnam National University, Ho Chi Minh City (VNU-HCM) under grant number DS2025-18-01. Hon Nhien Le was funded by the PhD Scholarship Programme of Vingroup Innovation Foundation (VINIF), VinUniversity, code VINIF.2025.TS13.

ABBREVIATIONS

SG: nanosilica derived from hydrogel
Cell: cellulose filter paper
SG/Cell: brush-coated nanosilica/cellulose membrane
MB: methylene blue trihydrate
MB1: methylene blue solution 1 ppm
MB20: methylene blue solution 20 ppm
SEM: scanning electron microscopy
EDS: energy-dispersive X-ray spectroscopy
XRD: X-ray diffraction
ATR FTIR: attenuated-total-reflectance Fourier-transform infrared spectroscopy
UV-Vis: ultraviolet-visible absorption spectroscopy
BET: Brunauer–Emmett–Teller theory
BJH: Barrett–Joyner–Halenda model
DFT: density functional theory
NLDFT: non-local density functional theory
dV-BJH: pore volume distribution derived from Barrett–Joyner–Halenda model

V-BJH: cumulative pore volume derived from Barrett–Joyner–Halenda model
dV-DFT: pore volume distribution calculated from density functional theory
V-DFT: cumulative pore volume calculated from density functional theory
STP: standard temperature and pressure
LMH: L m^{-2} h^{-1}
PES: polyethersulfone filter membrane
SPES: sufonated polyethersulfone filter membrane

CONFLICT OF INTEREST

The authors declare that they have no known competing financial interests or personal relationships that could have appeared to influence the work reported in this paper.

AUTHORS' CONTRIBUTIONS

Hon Nhien Le: Conceptualization; Methodology; Investigation; Formal analysis; Data curation; Visualization; Writing - original draft; and Writing - review & editing
Lam Nhu Pham: Experimental synthesis; Formal analysis; Investigation
Thi Bich Duyen Luu: Experimental synthesis; Formal analysis; Investigation
Thi Bang Tam Dao: Resources; Data curation
Trung Do Nguyen: Resources; Instrumentation
Chi Nhan Ha Thuc: Investigation; Supervision; Validation
Van Hieu Le: Funding acquisition; Project administration; Investigation; Supervision; Validation

REFERENCES

1. Yadav D, Rangabhashiyam S, Verma P, Singh P, Devi P, Kumar P, et al. Environmental and health impacts of contaminants of emerging concerns: recent treatment challenges and approaches. Chemosphere. 2021;272. Available from: https://doi.org/10.1016/j.chemosphere.2020.129492.
2. Hanafi MF, Sapawe N. A review on the water problem associate with organic pollutants derived from phenol, methyl orange, and remazol brilliant blue dyes. Materials Today: Proceedings. 2020;31:141–50. Available from: https://doi.org/10.1016/j.matpr.2021.01.258.
3. Jambeck JR, Geyer R, Wilcox C, Siegler TR, Perryman M, Andrady A, et al. Marine pollution. Plastic waste inputs from land into the ocean. Science. 2015;347(6223):768–71. Available from: https://doi.org/10.1126/science.1260352.
4. Sun J, Peng Z, Zhu ZR, Fu W, Dai X, Ni BJ. The atmospheric microplastics deposition contributes to microplastic pollution in urban waters. Water Research. 2022;225. Available from: https://doi.org/10.1016/j.watres.2022.119116.
5. Imbulana S, Tanaka S, Moriya A, Oluwoye I. Inter-event and intra-event dynamics of microplastic emissions in an urban river during rainfall episodes. Environmental Research. 2024;243. Available from: https://doi.org/10.1016/j.envres.2023.117882.
6. Zhang F, Xu K, Bai Y, Wang P. Multifunctional cellulose paper-based materials. Cellulose (London, England). 2023;30(14):8539–69. Available from: https://doi.org/10.1007/s10570-023-05426-y.
7. Azimi B, Sepahvand S, Ismaeilimoghadam S, Kargarzadeh H, Ashori A, Jonoobi M. Application of Cellulose-Based Materials as Water Purification Filters; A State-of-the-Art Review. Journal of Polymers and the Environment. 2024;32(1):345–66. Available from: https://doi.org/10.1007/s10924-023-02989-6.
8. Nhiên LH, Đặng Thị Minh Thư, Tiến LT, Đào Thị Băng Tâm, Độ NT, Nhân HTC. Nghiên cứu vật liệu nanosilica và than sinh học trích ly từ tro trấu từ lò hơi công nghiệp. Sci Tech Dev J - Nat Sci. 2025;7(S1):1–16. Available from: https://doi.org/10.32508/stdjns.v7iS1.1327;https://doi.org/10.32508/stdjns.v7iS1.1327.
9. Nhiên LH, Đào Thị Băng Tâm, Độ NT, Nhân HTC, An VN, Tốp LK, et al. Tổng hợp potassium silicate và than sinh học bằng phương pháp xử lý tro trấu trong dung dịch potassium hydroxide. Kỷ yếu Hội nghị Vật lý chất rắn và Khoa học vật liệu toàn quốc lần thứ 14 (SPMS 2025);.
10. Sun Y, Zhang Y, Yu W, Jia P, Zhang X, Wu N, et al. Bioinspired stretchable and self-healable nanocomposite gelatin hydrogel with low silica nanoparticle content and brilliant angle/strain-independent structural colors. Chemical Engineering Journal. 2024;496. Available from: https://doi.org/10.1016/j.cej.2024.154190.
11. Yeap SP. Permanent agglomerates in powdered nanoparticles: formation and future prospects. Powder Technology. 2018;323:51–9. Available from: https://doi.org/10.1016/j.powtec.2017.09.042.
12. Hochella MF, Mogk DW, Ranville J, Allen IC, Luther GW, Marr LC. Natural, incidental, and engineered nanomaterials and their impacts on the Earth system. Science. 2019;363(6434). Available from: https://doi.org/10.1126/science.aau8299.
13. Le HN, Nguyen DK, Dang MT, Nguyen HT, Dao TB, Nguyen TD, et al. Supramolecular hydration structure of graphene-based hydrogels: density functional theory, green chemistry and interface application. Beilstein Journal of Nanotechnology. 2025;16:806–22. Available from: https://doi.org/10.3762/bjnano.16.61.
14. Le HN, Nguyen TB, Nguyen DT, Dao TB, Nguyen TD, Thuc CNH. Sonochemical synthesis of bioinspired graphene oxide-zinc oxide hydrogel for antibacterial painting on biodegradable polylactide film. Nanotechnology. 2024;35(30). Available from: https://doi.org/10.1088/1361-6528/ad40b8.
15. Le HN, Dao TB, Nguyen TD, Dinh DA, Thuc CNH, Le VH. Revisiting oxidation and reduction reactions for synthesizing a three-dimensional hydrogel of reduced graphene oxide. RSC Advances. 2024;14(42):30844–58. Available from: https://doi.org/10.1039/D4RA05385K.
16. Le HN, Luu TB, Pham LN, Dao TB, Nguyen TD, Thuc CNH, et al. Scalable Syntheses of Graphene Oxide and Reduced Graphene Oxide using Cascade Design Oxidation and Highly Basic Reduction Reactions. Journal of Visualized Experiments. 2025;221(221). Available from: https://doi.org/10.3791/68313.
17. Le HN, Nguyen HD, Do MH, Nguyen TM, Nguyen TD, Dao TB, et al. Melt processing of graphene-coated polylactide granules for producing biodegradable nanocomposite with higher mechanical strength. Polymer-Plastics Technology and Materials. 2024;63(11):1421–37. Available from: https://doi.org/10.1080/25740881.2024.2335186.
18. Le HN, Thai D, Nguyen TT, Dao TB, Nguyen TD, Tieu DT, et al. Improving Safety and Efficiency in Graphene Oxide Production Technology. Journal of Materials Research and Technology. 2023;24:4440–53. Available from: https://doi.org/10.1016/j.jmrt.2023.04.050.
19. Klein J. Hydration lubrication. Friction. 2013;1(1):1–23. Available from: https://doi.org/10.1007/s40544-013-0001-7.
20. Ma L, Gaisinskaya-Kipnis A, Kampf N, Klein J. Origins of hydration lubrication. Nature Communications. 2015;6(1):6060. Available from: https://doi.org/10.1038/ncomms7060.
21. Han T, Zhang S, Zhang C. Unlocking the secrets behind liquid superlubricity: A state-of-the-art review on phenomena and mechanisms. Friction. 2022;10(8):1137–65. Available from: https://doi.org/10.1007/s40544-021-0586-1.

22. Ma P, Liu Y, Han K, Tian Y, Ma L. Hydration lubrication modulated by water structure at TiO2-aqueous interfaces. Friction. 2024;12(4):591–605. Available from: https://doi.org/10.1007/s40544-023-0750-x.
23. Adibnia V, Ma Y, Halimi I, Walker GC, Banquy X, Kumacheva E. Phytoglycogen nanoparticles: nature-derived superlubricants. ACS Nano. 2021;15(5):8953–64. Available from: https://doi.org/10.1021/acsnano.1c01755.
24. Kumar A, Kumar V, Joshi YM, Singh MK. Nano-silica based aqueous colloidal gels as eco-friendly thixotropic lubricant. Journal of Colloid and Interface Science. 2025;700(Pt 3). Available from: https://doi.org/10.1016/j.jcis.2025.138486.
25. Kumarage S, Munaweera I, Sandaruwan C, Weerasinghe L, Kottegoda N. Electrospun amine-functionalized silica nanoparticles–cellulose acetate nanofiber membranes for effective removal of hardness and heavy metals (As(V), Cd(II),Pb(II)) in drinking water sources. Environmental Science Water Research & Technology. 2023;9(10):2664–79. Available from: https://doi.org/10.1039/D3EW00312D.
26. Miri S, De Girolamo A, Nadeem H, Chin BW, Hora Y, Andrews PC. Composite membranes of cellulose–mesoporous silica: optimization of membrane fabrication and adsorption capacity. Cellulose (London, England). 2023;30(1):339–57. Available from: https://doi.org/10.1007/s10570-022-04908-9.
27. Joshi R, Sebat N, Chi K, Khan M, Johnson KI, Alhamzani AG. Low Fouling Nanostructured Cellulose Membranes for Ultrafiltration in Wastewater Treatment. Membranes (Basel). 2023;13(2):147. Available from: https://doi.org/10.3390/membranes13020147.
28. Ali AS, Soliman MM, Kandil SH, Ebrahim S, Khalil M. Tailoring nanocomposite membranes of cellulose acetate/silica nanoparticles for desalination. Journal of Materiomics. 2022;8(6):1122–30. Available from: https://doi.org/10.1016/j.jmat.2022.07.001.
29. Ding M, Lin B, Sui T, Wang A, Yan S, Yang Q. The excellent antiwear and friction reduction properties of silica nanoparticles as ceramic water lubrication additives. Ceramics International. 2018;44(12):14901–6. Available from: https://doi.org/10.1016/j.ceramint.2018.04.206.
30. Cui Y, Ding M, Sui T, Zheng W, Qiao G, Yan S. Role of nanoparticle materials as water-based lubricant additives for ceramics. Tribology International. 2020;142. Available from: https://doi.org/10.1016/j.triboint.2019.105978.
31. Rowe CD, Lamothe K, Rempe M, Andrews M, Mitchell TM, Toro GD. Earthquake lubrication and healing explained by amorphous nanosilica. Nature Communications. 2019;10(1):320. Available from: https://doi.org/10.1038/s41467-018-08238-y.
32. Le HN, Thuc CNH, Van HL. Advancements in chemical oxidation-reduction reactions and supramolecular hydrogels of graphene-based materials. Nanotechnology. 2025;36(50). Available from: https://doi.org/10.1088/1361-6528/ae1f23.
33. Carrillo F, Colom X, Suñol JJ, Saurina J. Structural FTIR analysis and thermal characterisation of lyocell and viscose-type fibres. European Polymer Journal. 2004;40(9):2229–34. Available from: https://doi.org/10.1016/j.eurpolymj.2004.05.003.
34. Hung DC, Nguyen NC, Uan DK, Son LT. Membrane processes and their potential applications for fresh water provision in Vietnam. Vietnam Journal of Chemistry. 2017;55(5):533. Available from: https://doi.org/10.15625/2525-2321.2017-00504.
35. Nhien LH, Dao TB, Hung DM, Bui TT, Do NT, Ha TC. Upgrading water purification membrane with photocatalytic and antibacterial coating of graphene oxide - zinc oxide nanocomposite. Vietnam Journal of Science and Technology. 2022;60:114–30. Available from: https://doi.org/10.15625/2525-2518/17151.
36. Nhien LH, Phat HT, Bui TT, Hung DM, Quoc LK, Ha TC. Synthesis of graphene oxide –gold nanobipyramids for antibacterial coating on water filtration membrane. Vietnam Journal of Science and Technology. 2022;60:1–14. Available from: https://doi.org/10.15625/2525-2518/16640.
37. Pieters K, Mekonnen T. Progress in waterborne polymer dispersions for coating applications: commercialized systems and new trends. RSC Sustainability. 2024;2(12):3704–29. Available from: https://doi.org/10.1039/D4SU00267A.
38. Saha A, Mishra P, Biswas G, Bhakta S. Greening the pathways: a comprehensive review of sustainable synthesis strategies for silica nanoparticles and their diverse applications. RSC Advances. 2024;14(16):11197–216. Available from: https://doi.org/10.1039/D4RA01047G.
39. Ghosh J, Rupanty NS, Noor T, Asif TR, Islam T, Reukov V. Functional coatings for textiles: advancements in flame resistance, antimicrobial defense, and self-cleaning performance. RSC Advances. 2025;15(14):10984–1022. Available from: https://doi.org/10.1039/D5RA01429H.
40. Horikawa T, Do DD, Nicholson D. Capillary condensation of adsorbates in porous materials. Advances in Colloid and Interface Science. 2011;169(1):40–58. Available from: https://doi.org/10.1016/j.cis.2011.08.003.
41. Virtanen T, Rudolph G, Lopatina A, Al-Rudainy B, Schagerlöf H, Puro L. Analysis of membrane fouling by Brunauer-Emmet-Teller nitrogen adsorption/desorption technique. Scientific Reports. 2020;10(1):3427. Available from: https://doi.org/10.1038/s41598-020-59994-1.
42. Ali H, Mansor ES, Taha GM. Microfiltration and adsorptive membranes for simultaneous removal of methyl orange and methylene blue using hybrid composites. Polymer Bulletin. 2022;79(9):7891–908. Available from: https://doi.org/10.1007/s00289-021-03884-7.
43. LaRue RJ, Warren A, Latulippe DR. Evaluation of microplastic particle transmission in a microfiltration process using fluorescence measurements: effect of pore size and flux. Journal of Membrane Science. 2024;708. Available from: https://doi.org/10.1016/j.memsci.2024.123045.
44. Chang ZH, Lyly LH, Teow YH, Yeap SP, Sum JY. Insight into polydopamine coating on microfiltration membrane with controlled surface pore size for enhanced membrane rejection. Polymer. 2023;287. Available from: https://doi.org/10.1016/j.polymer.2023.126446.
45. Al-Shaeli M, Smith SJ, Jiang S, Wang H, Zhang K, Ladewig BP. Long-term stable metal organic framework (MOF) based mixed matrix membranes for ultrafiltration. Journal of Membrane Science. 2021;635. Available from: https://doi.org/10.1016/j.memsci.2021.119339.